

# Exploiting arene-perfluoroarene interactions for dispersion of carbon black in rubber compounds

Prasad Raut <sup>a</sup>, Nicole Swanson <sup>b</sup>, Akshata Kulkarni <sup>a</sup>, Coleen Pugh <sup>b</sup>, Sadhan C. Jana <sup>a,\*</sup>

<sup>a</sup> Department of Polymer Engineering, University of Akron, Akron, OH, 44325, USA

<sup>b</sup> Department of Polymer Science, University of Akron, Akron, OH, 44325, USA

## ARTICLE INFO

### Article history:

Received 20 March 2018

Received in revised form

9 May 2018

Accepted 9 June 2018

Available online 14 June 2018

### Keywords:

Coupling agents

Dispersion

Carbon black

## ABSTRACT

Coupling agents are intended to promote filler dispersion by providing a bridge between the filler and the rubber phase. This study investigated the ability of a novel physical coupling agent, poly(butadiene-graft-pentafluorostyrene) in a mixture with polypentafluorostyrene, to improve rubber-filler interactions and suppress filler-filler networking in carbon-black-reinforced styrene-butadiene rubber (SBR), and thereby decrease hysteresis. The electron-rich aromatic rings of carbon black are involved in arene-perfluoroarene interactions with the electron-poor pentafluorostyrene aromatic rings of the coupling agent. The SBR chains in the rubber compound have an affinity for the polybutadiene backbone of the coupling agent. The interactions between carbon black and the coupling agent were analyzed using Raman spectroscopy, transmission electron microscopy, zeta potential measurements, surface area measurements, and scanning electron microscopy. Filler flocculation analysis showed that the coupling agent improves the dispersion and lowers the energy of dissipation. The hysteresis loss, quantified in terms of loss tangent values at 60 °C, was reduced by up to 12% due to the coupling agent's promotion of better filler-rubber interactions. The influence of the PPFS graft length was also studied.

© 2018 Elsevier Ltd. All rights reserved.

## 1. Introduction

The concept of rolling resistance is explained in various forms in the literature; one simple definition is the force required to make tires roll on road surfaces. According to the United States Department of Transportation, 240 million light trucks and passenger cars consume approximately 135 billion gallons of motor fuel each year in the United States [1]. In this context, rolling resistance is among several factors that determine the fuel economy. For example, approximately 2 billion gallons of fuel would be saved each year in the United States alone if the rolling resistance was decreased by 10% [2]. An improvement in fuel economy leads to reduced CO<sub>2</sub> emission and improved air quality.

The material packages used in tire tread formulations directly impact the rolling resistance (RR) of the resulting compounds. Two major avenues to improve the RR of tire tread compounds are the use of a rubber matrix with lower inherent values of RR and an increase of the rubber-filler interactions via the use of coupling agents. The first series of articles on filler-elastomer interactions

was published by Wang and coworkers [3,4]. These investigators explained the impact of filler-filler networks and surface energies of filler particles on dynamic mechanical properties of the compounds. Another approach to improve the dynamic mechanical properties is by controlling the filler microstructures [5] and filler dispersion [6]. For filled rubber systems, the loss ( $G''$ ) and storage ( $G'$ ) moduli values are determined from the state of filler networking along with hydrodynamic effects. The hydrodynamic effects depend strictly on the filler loading, while the values of  $G'$  are related to the filler networks that remain intact with the applied strain. The values of  $G''$ , however, are associated with the breakdown and reformation of filler-filler networks [7]. Luginsland et al. [8] reported that filler-filler interactions compete in both silica- and carbon black-filled systems.

A number of studies focused on increasing the rubber-filler interactions using covalent coupling agents in silica-filled rubber compounds [8–12]. Bis(triethoxysilylpropyl)tetrasulfide is a common covalent coupling agent for silica-filled rubber. In comparison, rubber-carbon black (CB) interactions did not receive much attention, except for studies involving nitroso compounds [13,14], unsaturated hydroxy organic acid [15], dinitroamines [16], dinitrodiamides [17], and isocyanates [18]. Nitroso compounds are

\* Corresponding author.

E-mail address: [janas@uakron.edu](mailto:janas@uakron.edu) (S.C. Jana).

carcinogenic with unfavorable health effects [5,19] while diamines more effectively enhance filler-polymer interactions compared to the dinitramides [17,20]. The isocyanate-based coupling agents require introduction of NCO groups onto carbon black surfaces. However, such groups are very sensitive to moisture and require further stabilization by masking the isocyanate groups by reversible addition of a weak acid across the N=C double bond [21].

This study introduces a novel physical coupling agent (CA) for carbon black (CB) based on arene-perfluoroarene interactions [22] between aromatic hydrocarbons and aromatic fluorocarbons. Arene-perfluoroarene interactions were first noted by Patrick and Prosser [21] when one equivalent of benzene ( $T_m = 5.5^\circ\text{C}$ ) mixed with one equivalent of hexafluorobenzene ( $T_m = 5^\circ\text{C}$ ) formed a transient complex that melted at  $24^\circ\text{C}$ , which is much higher than that of either component. Similarly, an equimolar solution of methylnaphthalene ( $T_m = 35^\circ\text{C}$ ) and hexafluorobenzene generate an isolatable crystalline complex that melts at  $56^\circ\text{C}$  [22]. The formation of these crystals was attributed to interaction of the electron-rich aromatic hydrocarbon and the electron-poor aromatic fluorocarbon. These arene-perfluoroarene interactions are a type of face-to-face  $\pi$ - $\pi$  stacking interactions that are used to provide physical crosslinks [23], aid in orienting reactants for polymerization [24] and photodimerization [25], and stabilize less ordered liquid crystalline phases [26].

As exemplified by the structure in Fig. 1, carbon black (CB) contains graphite-like microcrystalline substructures amongst its amorphous elemental carbon chemical make-up [27]. Most compounded rubber is reinforced with CB [28,29]. The graphitic content makes CB amenable to arene-perfluoroarene interactions with perfluoroarene materials. Paz-Pazos and Pugh reported the grafting of polybutadiene with 2,3,4,5,6-pentafluorostyrene using free radical initiation, to produce a mixture of the graft copolymer and polypentafluorostyrene homopolymer [30]. Fig. 2 presents a representative structure of the resulting PB-g-PPFS (polybutadiene-graft-polypentafluorostyrene) copolymer. The chemical structures of the copolymer's polybutadiene backbone and the rubber matrix are similar and will therefore interact well, while the electron-deficient pentafluorostyrene (PFS)  $\pi$ -system and the electron-rich graphitic CB can interact by arene-perfluoroarene interactions. This is the first study to exploit the physical, arene-perfluoroarene interactions to promote CB particle dispersion in rubber compounds. We recently demonstrated that the mixture of polybutadiene-graft-polypentafluorostyrene and PPFS is an effective coupling agent for improving the dispersion of polar hybrid lignin-coated carbon black particles in non-polar rubber [31].

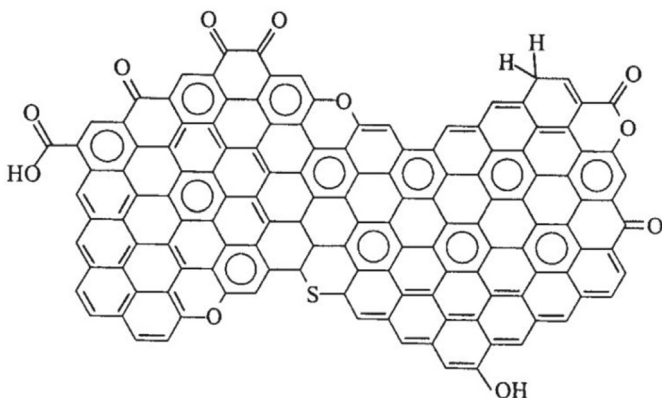


Fig. 1. Representative chemical structure of carbon black [32].

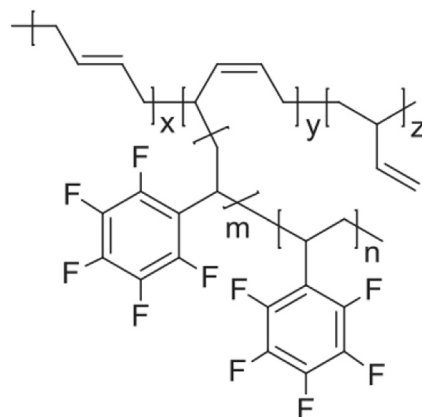


Fig. 2. Simplified structure of polybutadiene-g-polypentafluorostyrene (PB-g-PPFS).

## 2. Experimental

### 2.1. Materials

Butylated hydroxytoluene (BHT, Alfa-Aesar), carbon black (CB, donated by Eastman Chemical, grade N234), polybutadiene (BR donated by Goodyear; 0.8% 1,4-trans, 97.7% 1,4-cis, 1.5% 1,2-vinyl;  $M_n = 1.25 \times 10^5$  Da,  $\bar{D} = M_w/M_n = 4.6$ ), styrene-butadiene rubber (donated by Eastman Chemical Company (Akron, OH); 25 wt% styrene, 42 wt% vinyl content; grade BUNA VSL VP PBR 4041) were used as received. Antioxidant antiozonant PD2, *N*-(1,3-dimethylbutyl)-*N'*-phenyl-*p*-phenylenediamine and the ingredients used for rubber curing, *N*-*t*-butyl-2-benzothiazyl sulfenamide (TBBS) accelerator, Rubber Maker (sulfur curing agent), stearic acid (flakes), and zinc oxide (powder) were used as donated by Akrochem Corporation. Benzoyl peroxide (BPO, 97%, Aldrich) was stored at  $<-10^\circ\text{C}$  in a freezer after recrystallization in a refrigerator from 1:3 (v/v) chloroform/methanol. The inhibitor was removed from 2,3,4,5,6-pentafluorostyrene (Apollo Scientific) prior to each use by passing it through a small amount of basic activated alumina. Tetrahydrofuran (THF, reagent grade, Aldrich) used for polymerizations was dried and distilled under  $\text{N}_2$  from purple sodium benzophenone ketyl.

### 2.2. Synthesis of polybutadiene-graft-polypentafluorostyrene

PB-g-PPFS was synthesized by our previously reported route [30,31] using a constant 2:1 M ratio of PFS to PB repeat units. The temperature and the amount of initiator were varied to obtain different lengths of the PPFS grafts. In a custom-made round bottom flask sealed with a valve attached through a high vacuum joint, a THF solution of PB (1.2 g, 23 mmol butadiene groups) was deoxygenated by 5 freeze-evacuate-thaw routines. The mixture was stirred overnight at  $50^\circ\text{C}$  in a  $\text{N}_2$  atmosphere to fully dissolve PB. Benzoyl peroxide (0.55 g, 2.3 mmol) and PFS (8.8 g, 45 mmol) were added to the PB soln. at room temperature, and the solution was again deoxygenated by 5 freeze-evacuate-thaw routines. After stirring at  $60^\circ\text{C}$  under a 1 mm Hg vacuum for 48 h, the graft copolymerization was terminated by opening the flask to air after cooling it to  $0^\circ\text{C}$ . In order to prevent oxidative crosslinking of the isolated PB-based graft copolymer, the polymerization solution was precipitated into a solution of BHT (1% w/v) in methanol (500 mL) saturated with  $\text{N}_2$ . The resulting white solid (7.3 g, 73% yield) contained PB-g-PPFS graft copolymer ( $M_n = 398$  kDa,  $\bar{D} = 1.63$ ), PPFS homopolymer ( $M_n = 8.52$  kDa), and a negligible quantity of unreacted PB homopolymer. This mixture of PB-g-PPFS and PPFS

homopolymer was used without further purification to prepare the hybrid CB:PB-g-PPFS filler.

### 2.3. Treatment of filler particles with CA

Both CB and PB-g-PPFS (CA) were available in particulate forms. We, therefore, prepared CA-coated CB particles by dispersing CB particles in a solution of CA. CB particles were added to a THF solution of CA at 50 °C, and the mixture was stirred on a hot plate for 2 h. The CA-coated CB particles were recovered by evaporating THF on the hot plate at 80 °C, and then drying in a vacuum oven at 80 °C. The agglomerated particles were milled to a size smaller than 100 μm.

### 2.4. Preparation of SBR rubber compounds

Compounds were prepared with and without the coupling agent (CA) by a two-step process using a Brabender Plasticorder internal mixer (85 cm<sup>3</sup>) first and then a two-roll mill. The components were mixed in the Brabender mixer at 65 rpm with a starting temperature of 80 °C and a 0.7 fill factor. A portion of the carbon black (1/2) was added to the rubber after masticating it for 1 min, followed by the rest of the carbon black that had been mixed for 3 min with processing oil. Antioxidant, ZnO and stearic acid were added late in the mixing cycle (7-min total mixing time). The compounds obtained from the internal mixer were mixed with sulfur and TBBS for 5–7 min at 50 °C using a two-roll mill at a 20 rpm roll speed.

The compounds were molded and cured at 160 °C under 25 MPa compression using a Wabash hydraulic press. A mold of dimension 15 cm × 15 cm × 2 mm was used for this purpose. The time required for curing was estimated using a moving die rheometer (MDR). Table 1 lists the recipes of the compounds. The number specified in parenthesis for formulation 2, 3 and 4 (5.5 kDa, 8.5 kDa and 14.5 kDa, respectively) represents the molecular weight of the PPFS graft. The amount of CA in the recipe was set at 4 phr in an ad-hoc manner. A future study will investigate the sensitivity of the data to other content of CA.

## 3. Characterization

### 3.1. GPC characterization

The polystyrene-equivalent molecular weights of the graft copolymers were analyzed at 35 °C using Millenium Empower 3 software and a gel permeation chromatography (GPC) instrument consisting of THF eluting at 1 mL/min, a guard column, a bank of Millipore linear (50–10<sup>4</sup> Å), 50 Å, 100 Å, 500 Å and 10<sup>4</sup> Å columns, and Waters 486 UV/Vis (254 nm) and 410 RI detectors.

### 3.2. NMR spectroscopic characterization

The structure of the graft copolymers was confirmed by <sup>19</sup>F (297 MHz) and <sup>1</sup>H (300 MHz) NMR spectroscopy using a Varian Mercury 300 spectrometer. The spectra (δ, ppm) of the samples dissolved in CDCl<sub>3</sub> were recorded relative to resonances of residual solvent referenced to trifluoroacetic acid (CF<sub>3</sub>COOH, –78.50 ppm) and SiMe<sub>4</sub> (TMS, 0.00 ppm), respectively.

### 3.3. Raman spectroscopic characterization

The CA:CB particles and their two components were characterized by Raman spectroscopy using a high-resolution Horiba Scientific LabRAM HR800 Raman spectrometer with a Synapse CCD detector. For Raman analysis, CA-coated CB particles with 1:1 CB:CA by weight were prepared by adding CB to an equal amount of PB-g-PPFS dissolved in THF. After evaporating THF from the solution on a hot plate, the particles were dried at 80 °C with a vacuum. The images were recorded using a 50 objective lens and a 532.07 nm laser excitation length. The spectra obtained were normalized to estimate the ratio of the peak intensities.

### 3.4. Morphological analyses

Transmission electron microscope (TEM) images of CA-coated CB particles and neat CB were recorded using a JEOL JSM-1230 TEM and a 300-mesh copper grid at a voltage of 120 kV. Scanning electron microscopy of these samples was performed on the JEOL JSM5310 with an operating voltage of 10 kV using carbon tape mounted on aluminum stubs. CB particles were added to a solution of graft copolymer in THF, and after ultrasonication for 3 min, the mixture was stirred for 6 h, and centrifuged at 9000 RPM for 40 min. After diluting (1:10 ratio) with THF, one drop of the supernatant was cast onto a TEM copper grid (300-mesh) for TEM imaging. After drying, the settled particles were imaged by SEM using a JEOL JSM5310 electron microscope. The quality of particle dispersion in the rubber compounds was determined from SEM images. For this purpose, vulcanized samples were cut into pieces and freeze-fractured using liquid nitrogen. The fractured surfaces were sputter coated with silver for 1.5 min under argon. The SEM voltage was varied from 5 kV to 10 kV.

### 3.5. Zeta potential measurements

The zeta potentials of suspensions of carbon black in tetrahydrofuran, and of carbon black in a tetrahydrofuran solution of the graft copolymer were measured using a ZETAPALS analyzer (640 nm, 35 mW red diode laser, Brookhaven, USA). For this

**Table 1**

Recipes used to prepare SBR compounds.<sup>a</sup> The molecular weight of PPFS graft in kDa in the coupling agents (CA) are presented in the parenthesis.

Formulation	1	2	3	4
	CB (phr)	CB-CA (5.5 kDa) (phr)	CB-CA (8.5 kDa) (phr)	CB-CA (14.5 kDa) (phr)
SBR	70	70	70	70
BR	30	30	30	30
CB	50	50	50	50
PB-g-PPFS	–	4	4	4
Stearic Acid	2	2	2	2
ZnO	2.5	2.5	2.5	2.5
TDAE <sup>b</sup>	15	15	15	15
A.O. (antioxidant)	1	1	1	1
TBBS	2	2	2	2
SULFUR	1.5	1.5	1.5	1.5

<sup>a</sup> Amounts given in parts per hundred rubber (phr).

<sup>b</sup> Processing oil.

**Table 2**  
Reaction conditions and resulting molecular weight characterization of the poly(butadiene-*graft*-pentafluorostyrene) copolymers.

PFS: PB Molar Ratio	mol% BPO	Reaction Time (h)	Reaction Temperature (°C)	Reaction % Yield	PB-g-PPFS $M_n \times 10^{-5}$ (Da)	PB-g-PPFS Đ	PPFS $M_n \times 10^{-3}$ (Da)
2: 1	10	60	80	87	3.76 <sup>a</sup>	2.35	5.10
2: 1	10	48	60	73	3.98	1.63	8.52
2: 1	5	48	60	46	5.34	1.61	14.5

<sup>a</sup> GPC analysis without the linear (50–10<sup>4</sup> Å) Millipore column in GPC instrument.

purpose, CB particles (50 ppm) were dispersed in THF and an appropriate amount of PB-g-PPFS was added to obtain 1:1 by weight of CB and CA. The suspension was sonicated to completely disperse the particles, and then the suspension was filtered through a grade 2 filter paper (8 μm pore size) to remove large CB agglomerates and any insoluble solids. For neat samples, 50 ppm CB was sonicated in THF for complete dispersion.

### 3.6. BET surface area measurements

Nitrogen adsorption-desorption isotherms from a Micromeritics Tristar II 3020 analyzer were used to measure the BET surface areas of CA-coated and non-treated CB at 77 K. The N<sub>2</sub> sorption analyses were performed on samples that had been degassed for 12 h at 60 °C.

### 3.7. Characterization of cure

The cure curves were obtained using an MDR 2000 moving die rheometer at 160 °C using a 7% strain and frequency of 1.67 Hz. For this purpose, ~5 g rubber compound was used. The cure time ( $t_{95}$ ) corresponding to the time to reach a torque of 95% ( $S_{95}$ ) was estimated from the raw data of torque vs. time plot. The torque  $S_{95}$  was calculated using equation (1).

$$S_{95} = S_{min} + 0.95 \times (S_{max} - S_{min}) \quad (1)$$

In equation (1),  $S_{min}$  is the minimum value and  $S_{max}$  is the maximum value of torque during the curing [33].

### 3.8. Dynamic mechanical analysis

The dynamic mechanical properties of 9 × 3.18 × 2 mm samples

were characterized using a TA Instruments DMA Q800. A uniform width of the sample was ensured by cutting cured sheets using an ASTM-D638 type V die. After establishing the linear-viscoelastic region by performing a strain sweep experiment at 1 Hz, a temperature sweep experiment was performed from –90 to 150 °C at 3 °C/min, 1 Hz frequency and 0.5% strain.

### 3.9. Mechanical property measurements

Tensile testing was performed on five specimens of the cured samples using an Instron<sup>®</sup> 5567 tensile tester equipped with an extensometer at a 500 mm/min crosshead speed. Cured sheets were cut into dumb-bell shaped specimens using ASTM-D412, Type-C die. Rubber sheets were cured at 160 °C in a compression mold at 25 MPa pressure for the amount of time estimated from the MDR cure curve.

### 3.10. Characterization of filler flocculation and the Payne effect

The filler flocculation behavior and nonlinear behavior of the storage modulus under high strain (Payne effect) were studied at the curing temperature (160 °C) of the rubber compound using an APA-2000 advanced polymer analyzer (Alpha Technologies). The rubber compounds contained no curatives. A sample was first strained at 25% for 5 min to remove pre-mixing influences on filler aggregation. The storage modulus values at 1% strain were then recorded for a period of 2 h. The Payne effect was studied by subjecting the materials to a strain sweep in the range of 0.13–70% strain after the filler flocculation test sequence was completed.

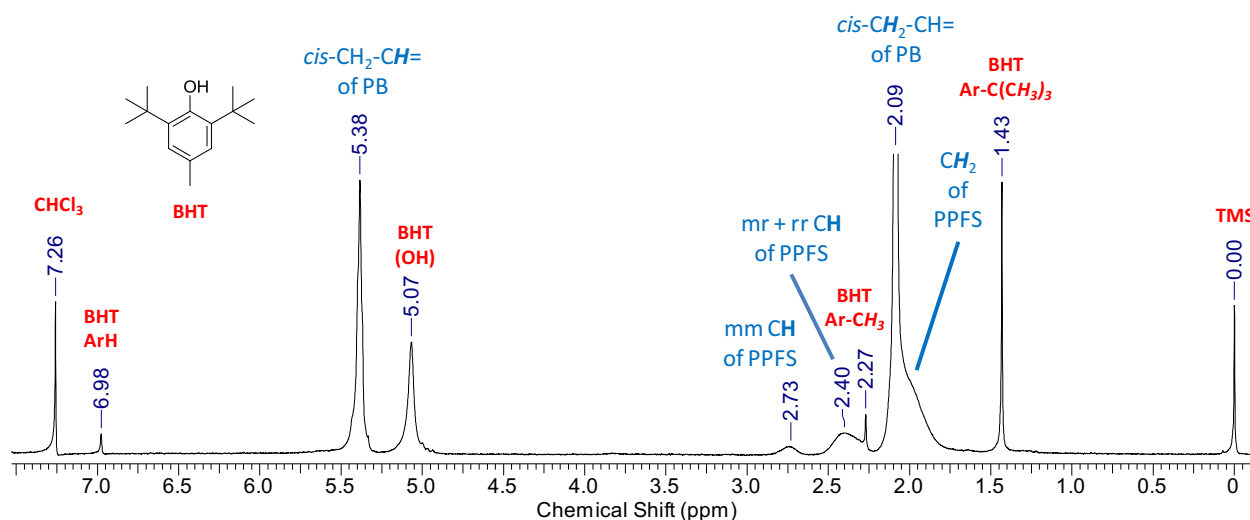


**Fig. 3.** 300 MHz <sup>1</sup>H NMR spectrum of a mixture of poly(butadiene-*graft*-pentafluorostyrene) and poly(pentafluorostyrene) generated by graft copolymerization. A negligible quantity of unreacted PB may also be present. BHT was added to prevent oxidative crosslinking of the PB units.

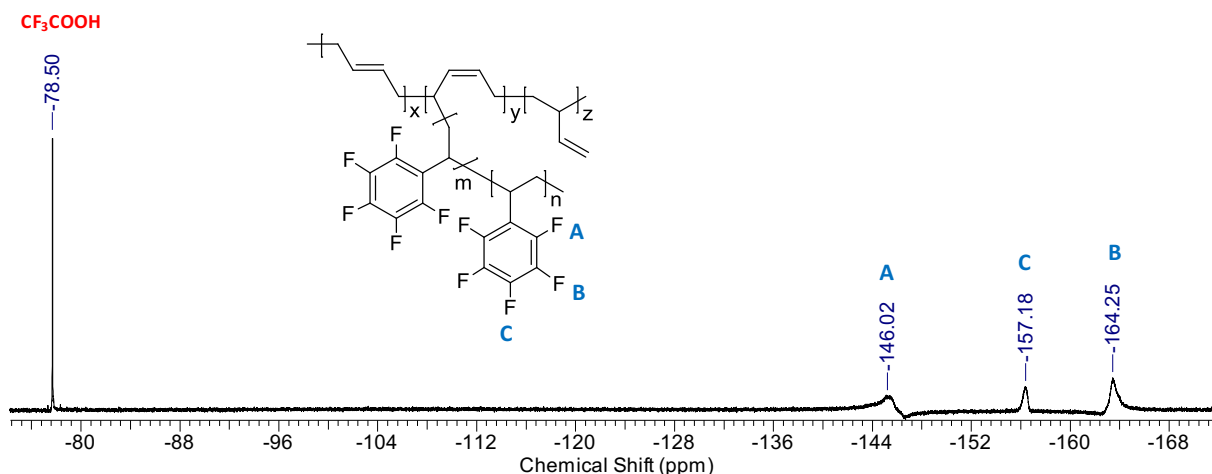


**Fig. 4.** 297 MHz  $^{19}\text{F}$  NMR spectrum of the mixture of poly(butadiene-*graft*-pentafluorostyrene) copolymer and PPFS homopolymer generated by graft copolymerization; referenced to trifluoroacetic acid.

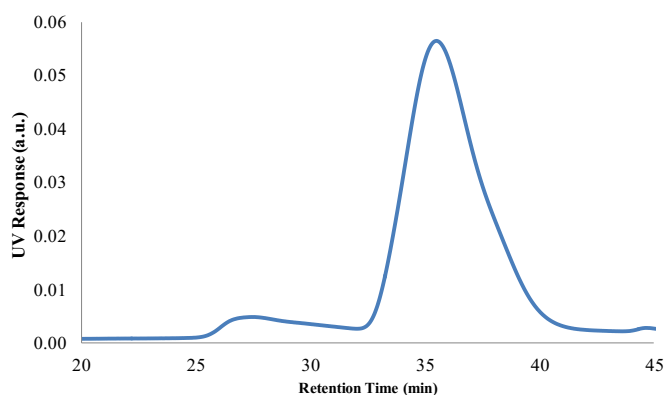


**Fig. 5.** UV-detected gel permeation chromatogram of poly(butadiene-*graft*-pentafluorostyrene) and PPFS homopolymer produced at 48 h.

## 4. Results and discussion

### 4.1. Synthesis and structural and molecular weight characterization of poly(butadiene-*graft*-pentafluorostyrene)

As listed in Table 2, the molecular weights of the PPFS homopolymer and the corresponding PPFS grafts in the copolymers were varied from  $5.10 \times 10^3$  Da to  $1.45 \times 10^4$  Da by varying the reaction temperature and the molar ratio of the initiator (benzoyl peroxide) with respect to PFS and PB content. Since a low concentration of initiator was used, the rates of growth and termination are the same for the free and grafted PPFS chains, thereby producing free homopolymer and graft copolymer with similar PPFS average lengths [30].

Fig. 3 presents the  $^1\text{H}$  NMR spectrum of a representative graft copolymer. The PB backbone resonances and the resonances from the PPFS homopolymer and PB-*g*-PPFS graft copolymer are evident. Paz-Pazos and Pugh [30] confirmed the formation of the graft copolymer by isolating both the copolymer and the PPFS homopolymer from the crude mixture. The  $^1\text{H}$  NMR resonances of the crude mixture shown in Fig. 3 correspond to the spectrum of isolated graft copolymer [30]. The resonances (ppm) due to protons in PB-*g*-PPFS chains are identified as follows: PPFS  $\text{CH}_2$  (2.00), PB *cis*- $\text{CH}_2$ - $\text{CH}=\text{}$  (2.09), PPFS heterotactic and syndiotactic  $\text{CH}$  dyads (2.40), PPFS isotactic  $\text{CH}$  dyads (2.73), PB *cis*- $\text{CH}_2$ - $\text{CH}=\text{}$  (5.38). The resonances corresponding to the added antioxidant BHT are also detectable at 1.47 ppm (*t*-Bu  $\text{CH}_3$ ), 2.47 ppm (Ar $\text{CH}_3$ ) 5.07 ppm ( $\text{OH}$ ) and 6.98 ppm (aromatic protons).

Fig. 4 presents the  $^{19}\text{F}$  NMR spectrum of the PB-*g*-PPFS-60/5/48 product. The fluorine atoms resonate at  $-146.0$  ppm (*F* *ortho* to the backbone),  $-164.3$  ppm (*F* *meta* to the backbone) and  $-157.2$  ppm (*F* *para* to the backbone). This spectrum is consistent with that reported previously [30].

As demonstrated by the GPC chromatograms presented in Fig. 5 and Figure S3 of the supporting information, the crude graft copolymers have bimodal molecular weight distributions with a high molecular weight graft copolymer eluting at lower volume and a lower molecular weight PPFS homopolymer eluting at higher volume. The trace amounts of unreacted PB (<5% [30]) are not noticeable at the UV detector response scale of PPFS. Prior to analyzing the graft copolymers, the UV detector was calibrated for PPFS concentration at 254 nm using the area under the peak in the GPC chromatograms of PPFS homopolymer, according to a previously reported procedure [30]. The areas under the low volume and high volume peaks in the GPC chromatograms of the crude graft copolymers correspond to the amount of PPFS grafted onto PB and the amount of homopolymerized PPFS, respectively.

**Table 3**

Grafting parameters of the poly(butadiene-*graft*-pentafluorostyrene) copolymers.

PPFS $M_n \times 10^{-3}$ (Da)	PB- <i>g</i> -PPFS $M_n \times 10^{-5}$ (Da)	PB- <i>g</i> -PPFS Đ	% PFS Conversion	Grafting Ratio (wt/wt)	Grafting Efficiency (%)	Grafting Frequency
5.10	3.76 <sup>a</sup>	2.35	77	0.48	8.9	193
8.52	3.98	1.63	87	0.39	6.2	406
14.5	5.34	1.61	48	0.18	5.3	1513

<sup>a</sup> GPC analysis without linear (50-10<sup>4</sup> Å) Millipore column in GPC instrument.

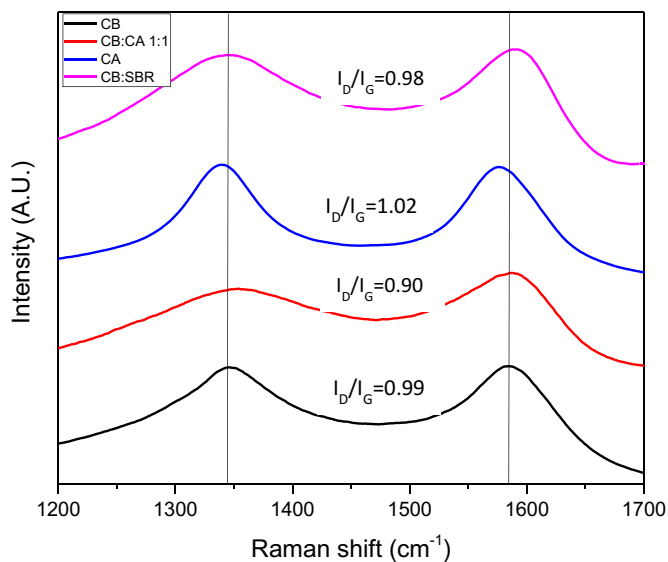


Fig. 6. Raman spectra of CB, CA, CA-coated CB particles (CB:CA) and SBR-coated CB particles (CB:SBR).

Table 3 summarizes the grafting parameters from this graft copolymerization using the area from the GPC chromatograms. Using both peaks in the chromatogram, the total mass of PPFS was divided by the original amount of monomer used in the copolymerization to calculate the monomer conversion. The grafting ratio equals the mass of grafts (grams of PPFS) per mass of polybutadiene

backbone (grams of PB). The grafting efficiency equals the wt% of PPFS that has been grafted onto PB. The grafting frequency equals the average number of butadiene repeats separating the graft sites. With increasing length of the PPFS graft, the graft ratio, efficiency, and frequency decreased. The molecular weight and length of the graft (and homopolymer) increased when less BPO initiator was used (Table 1) and therefore, fewer graft sites were generated, which also corresponded to higher graft frequency.

#### 4.2. Raman spectroscopic characterization of the particles and curing agents

The Raman spectra of neat CB particles, CA-coated CB particles, SBR-coated CB particles, and neat CA are presented in Fig. 6. The 532-nm excitation laser creates a peak at approximately  $1580\text{ cm}^{-1}$  corresponding to the G-band vibrations of the graphite crystal lattice. The  $1350\text{ cm}^{-1}$  peak is called the D-band; it arises due to disorder in the graphitic crystal lattices [34,35]. These defects exist mostly at the edges of the graphite crystals [36,37]. The level of disorder in the graphitic crystal lattice of CB can be characterized by monitoring the  $I_D/I_G$  ratio of the intensities of the D-band and G-band. As seen in Fig. 6, the CA-coated CB particles show lower  $I_D/I_G$  ratio,  $\sim 0.90$  compared to SBR-coated CB particles (0.98) and neat CB (0.99). Such a reduction in  $I_D/I_G$  ratio for CA-coated CB particles is attributed to more effective CB-CA interactions via  $\pi$ - $\pi$  stacking. The highest concentration of  $\pi$ -electrons is found at or around the edges of the crystallites (defect/disordered areas) [38]. Similar inferences were drawn for arene-perfluoroarene interactions in the case of CNT-sodium lignosulfonate [39] and lignin-CB [36] systems. The D and G-bands of the CA-coated CB particles also shift to higher

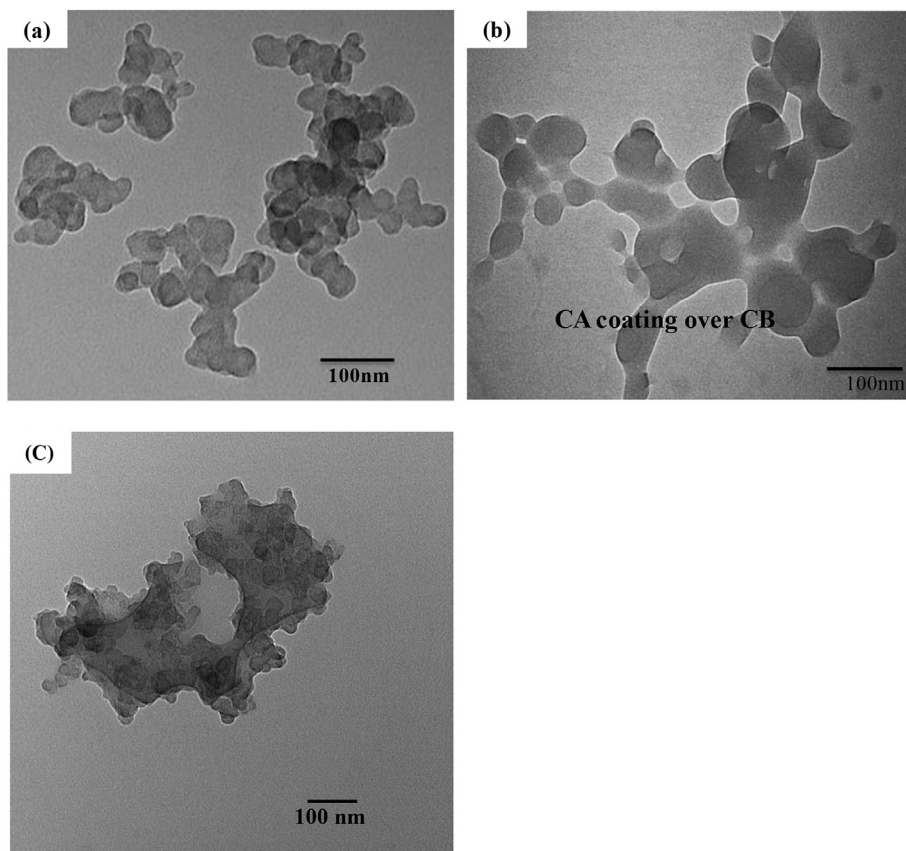
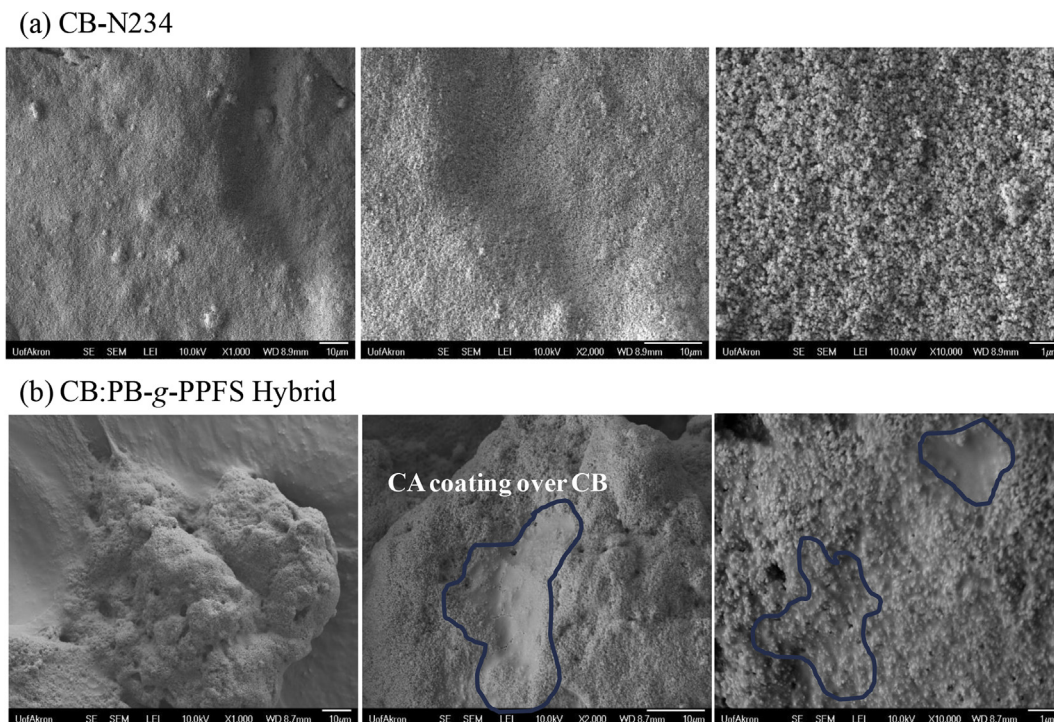


Fig. 7. TEM pictures of (a) carbon black, (b) 1:1 w/w carbon black:poly(butadiene-graft-pentafluorostyrene), and (c) 1:1 w/w carbon black:SBR drop-cast from 0.01% THF solutions.



**Fig. 8.** SEM pictures of carbon black particles (a), and a hybrid of CB and PB-g-PPFS (b); a carbon black coated with PB-g-PPFS coupling agent is outlined in (b).

wavenumbers. For example, the D-band shifted from  $1345.4\text{ cm}^{-1}$  in CB to  $1353.6\text{ cm}^{-1}$  in CA-coated CB, while the G-band shifted from  $1584.1\text{ cm}^{-1}$  in CB to  $1586.1\text{ cm}^{-1}$  in CA-coated CB. The shift to higher wavenumber indicates that higher energy is required to sustain the vibrations of groups engaged in arene-perfluoroarene interactions. The higher shift in the D-band also indicates that PPFS interacts with graphite at the crystallite edges of CB due to the higher local concentration of the  $\pi$ -bonds.

#### 4.3. Morphological evidence of interactions between the coupling agent and carbon black

The ability of the electron-deficient PFS aromatic rings of the copolymer to form arene-perfluoroarene interactions with electron-rich carbon black by  $\pi$ - $\pi$  stacking was investigated by TEM. A drop of a dilute suspension of 1:1 w/w CB and the graft copolymer/PPFS mixture in tetrahydrofuran was cast onto a TEM grid. Fig. 7(a) shows that the CB particles have a primary particle size of  $\sim 25\text{ nm}$ , and form aggregates with sizes of  $100\text{--}150\text{ nm}$ . The TEM image in Fig. 7(b) shows that PPFS chains of the graft- and homopolymers coated the CB particles uniformly and that the fractal nature of CB particles was retained. This uniform coating of CA over CB should reduce the filler networking by preventing CB particles from coming into contact with each other. The thickness of the coating layers cannot be inferred from this TEM image due to the similar electron density of PB-g-PPFS and CB primary particles. Similarly, a solution of SBR and CB was prepared and the TEM image was taken after drop casting on a TEM grid as shown in Fig. 7(c). It appears that SBR formed thin layers on CB particles and not all CB particles, especially at the edges, were coated with SBR.

Fig. 8 compares the SEM images of CB and CA-coated CB particles. These SEM images demonstrate that the morphology of the porous ensemble of CB particles changed significantly by coating with the coupling agent.

#### 4.4. Zeta potentials of treated and untreated carbon black particles

Table 4 shows the zeta potentials of carbon black dispersed in THF in the presence and absence of dissolved coupling agent. The data were collected at the same particle loadings ( $50\text{ ppm}$ ) at  $25\text{ }^\circ\text{C}$ . The zeta potential of carbon black particles dispersed in THF increased from  $-17.52 \pm 2.46\text{ mV}$  for neat CB to  $-4.90 \pm 2.14\text{ mV}$  in the presence of the graft copolymer. The surface charges on particles originate from ionization of surface groups, loss of ions, or adsorption of species. CB particles have several functional groups, including phenols, carboxylic acids, lactones and quinones [40]. Dissociation of the acid groups on the particle surface gives rise to a negative potential. Xu et al. [41] observed that CB behaved as a Lewis acid with a negative zeta potential in polar or semipolar solvents (dielectric constant  $< 33$ ). The increased zeta potential of the THF solution of CB particles in the presence of the graft copolymer is evidently due to coverage of their functional groups

**Table 4**

Zeta potential values at  $25\text{ }^\circ\text{C}$  of untreated carbon black and carbon black treated with PB-g-PPFS.

Specimen in THF	Zeta Potential (mV)
carbon black	$-17.52 \pm 2.46$
CB with dissolved CA	$-4.90 \pm 2.14$
CB with dissolved SBR	$-0.39 \pm 1.89$

**Table 5**

BET surface area of neat carbon black and CB particles treated with PB-g-PPFS.

Sample	BET Surface Area ( $\text{m}^2/\text{g}$ )
CB	108.2
CB:CA (1:1)	70.1
CB:SBR (1:1)	91.3

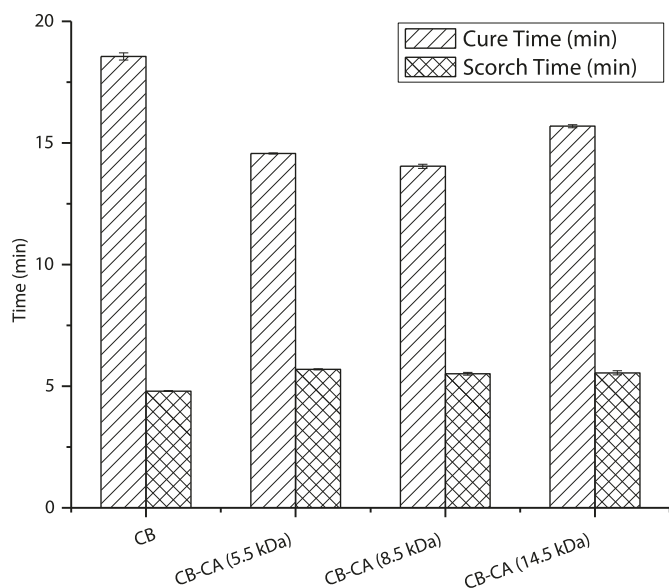


Fig. 9. Cure and scorch times of rubber compounds with and without CA.

by adsorbed PB-g-PPFS molecules, as was already established in the solid state by the TEM image in Fig. 7. The zeta potential value of CB-SBR was  $-0.39 \pm 1.89$  mV. One may be tempted to infer that CB-SBR interactions in THF solution were stronger than CB-CA interactions. However, one cannot draw any conclusion on relative strength of the interactions due to large standard deviation values in both cases. We, however, note that 1 g of SBR contained 22 mol% more styrene repeat unit than 1 g of PB-g-PPFS. Thus, SBR can interact with CB using 22 mol% more styrene.

#### 4.5. BET surface area of treated and untreated carbon black particles

Table 5 summarizes the surface area values of untreated carbon

black and CA-coated carbon black particles. The surface area of CB was reduced by 35% after coating the particles with the graft copolymer mixture, which evidently blocked access of  $N_2$  gas to the porous area of CB. The surface area for SBR-treated CB particles represents a 15% reduction, indicating much less coverage of the pores of CB particles by SBR chains than the graft copolymer.

#### 4.6. Curing of the rubber compounds

Rubber compounds were prepared using the four different formulations summarized in Table 1. Formulation (1) used neat CB as a control batch, and formulations (2), (3), and (4) contained the graft copolymer/PPFS coupling agent with different PPFS graft lengths. The curing behavior was characterized at  $160^\circ\text{C}$  using MDR. Fig. 9 presents the cure and scorch times of compounds of carbon black and CA-coated CB. The values of  $t_{95}$ , i.e., the time corresponding to 95% of the torque value, are shown. The neat CB compounds cured in  $\sim 18.5$  min, which is similar to that of the TBBS sulfur cure package. All of the compounds containing the coupling agent cured in less time. It is widely accepted in the literature that CB particles act as a catalyst in the vulcanization system [42–45]. The reduced curing time is therefore consistent with enhanced filler dispersion, which results in greater CB surface area available to catalyze vulcanization. It is apparent from the data presented in Fig. 9 that all three coupling agents reduced the curing time, with the two lowest molecular weight samples 5.5 kDa and 8.5 kDa showing the greatest effect. It is apparent that the difference in molecular weight of the above two coupling agent specimens was not large enough to see a significant difference in the curing time as was seen in the case of coupling agent of much higher molecular weight of 14.5 kDa. The scorch time increased by more than 1 min in compounds containing the CA, indicating higher processing times for these compounds. The scorch time is a measure of the onset of crosslinking [46]. For polar filler particles, the vulcanization chemicals are adsorbed on the surfaces of CB during mixing, which delays vulcanization [47]. The higher scorch times of CA-containing compounds compared to the control material indicates that the coating of PPFS onto CB (see Fig. 7) increases its polarity, possibly

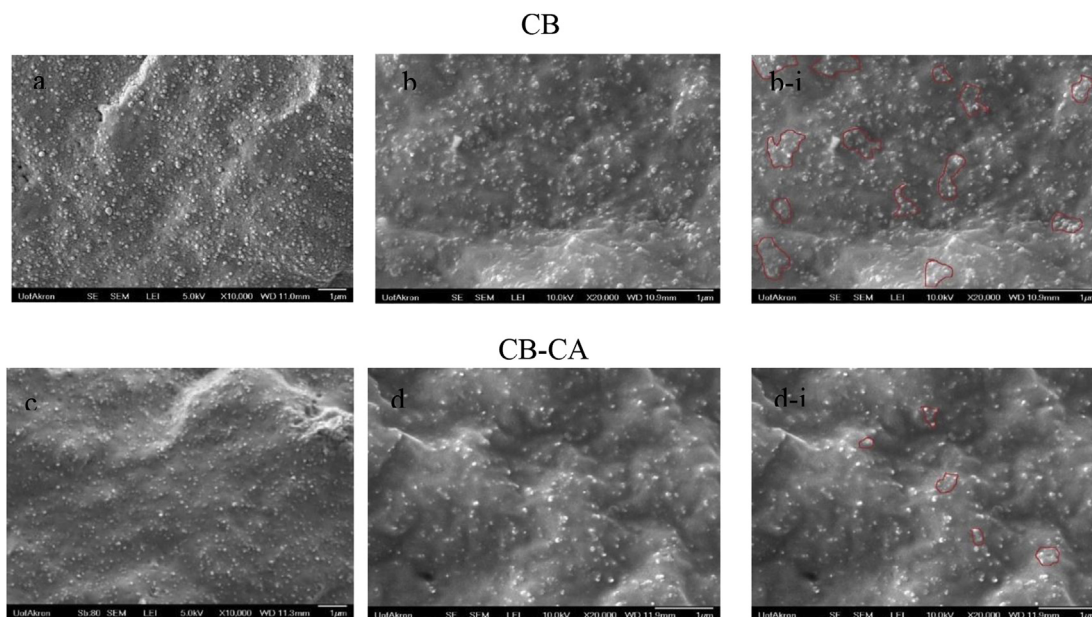


Fig. 10. SEM pictures of fractured surfaces of rubber compounds containing carbon black (a, b, b-i) and carbon black coated with coupling agent (8.5 kDa) (c, d, d-i). Images b-i and d-i have outlined the CB domains of b and d, respectively. CB domains highlighted.

due to the electronegative fluorine atoms in the perfluoroarene rings.

#### 4.7. CB particle dispersion from scanning electron microscopy

SEM pictures of the fractured rubber surfaces were recorded to determine how the coupling agent affected the morphology of the cured compounds. Comparison of the SEM images 'a' and 'c' in Fig. 10 demonstrates that the coupling agent led to better dispersion of CB particles and reduction of their aggregate size. The lower area density of particle aggregates in images Fig. 10(c)–(d) indicates dispersion of higher fractions of CB particles in rubber. The reduced aggregate size is especially visible when the magnification is doubled in images 'b' and 'd'; some representative CB regions are outlined in b-i and d-i. We attribute better CB dispersion in the compounds containing the coupling agent to the arene-perfluoroarene interactions between CB and the pentafluorostyrene rings of PB-g-PPFS and PPFS.

#### 4.8. Dynamic mechanical properties of the compounds

The dynamic mechanical properties of the rubber compounds were determined in tension mode using a temperature sweep in their linear viscoelastic regime. Representative data sets are included in Figure S2. Fig. 11 presents the values of  $\tan \delta$  and the storage modulus of the materials obtained with coupling agents. At 60 °C, the  $\tan \delta$  value serves as an indicator of the viscous dissipation and a rolling resistance indicator of the compound [48]. At 0 °C, the  $\tan \delta$  value serves as an indicator of the wet skid resistance [49]. The data presented in Fig. 11(a) demonstrate that all compounds containing the CA show lower mean values of  $\tan \delta$  and, therefore, lower hysteresis loss at 60 °C compared to those with no coupling agent. This is more apparent for CA molecules with graft molecular weight 5.5 kDa and 8.5 kDa, although the data for CA with 5.5 kDa graft molecular weight show larger error bar. We infer that the PB backbone and the PPFS graft in CA provide a physical link between CB particles and the elastomer matrix, which in turn, leads to enhanced rubber–filler interactions resulting in a lower  $\tan \delta$  value at 60 °C. These values increase with increasing molecular weight of the PPFS graft, indicating that shorter graft chain length is more effective at increasing rubber–filler interactions.

The wet skid resistance indicator,  $\tan \delta$  at 0 °C, of the compounds containing coupling agents show more significant improvement than  $\tan \delta$  values at 60 °C. For example,  $\tan \delta$  at 0 °C increased with an increase of graft molecular weight compared to the control materials. Thus, we infer that the compounds with CA are more suited to offer higher wet-skid resistance than the control.

The trend of  $\tan \delta$  at 0 °C data is attributable to phase separation of the PPFS grafts from PB. For neat solution-cast PB-g-PPFS (supporting info), PPFS forms microphase separated domains. The domain size should increase with increasing molecular weight of the graft. Since PB is an inherent part of the matrix, the PB backbone is miscible with the rubber matrix. Phase separation of the PPFS grafts contributes to additional rubber domains to the whole rubbery matrix, thereby increasing the loss modulus for the overall compounds.

The storage modulus values at 0 °C for materials with coupling agents show reduction from a mean value of about 32 MPa of the control material to 28, 25, and 30 MPa for compounds with coupling agents of graft molecular weight 5.5, 8.5, and 14.5 kDa respectively. The storage modulus values measured at 60 °C show similar trend with mean values of 12.5, 10, 8, and 12 MPa respectively for control and compounds with coupling agents of graft molecular weight 5.5, 8.5, and 14.5 kDa. These data indicate that the addition of coupling agents caused a reduction of the stiffness of the compounds.

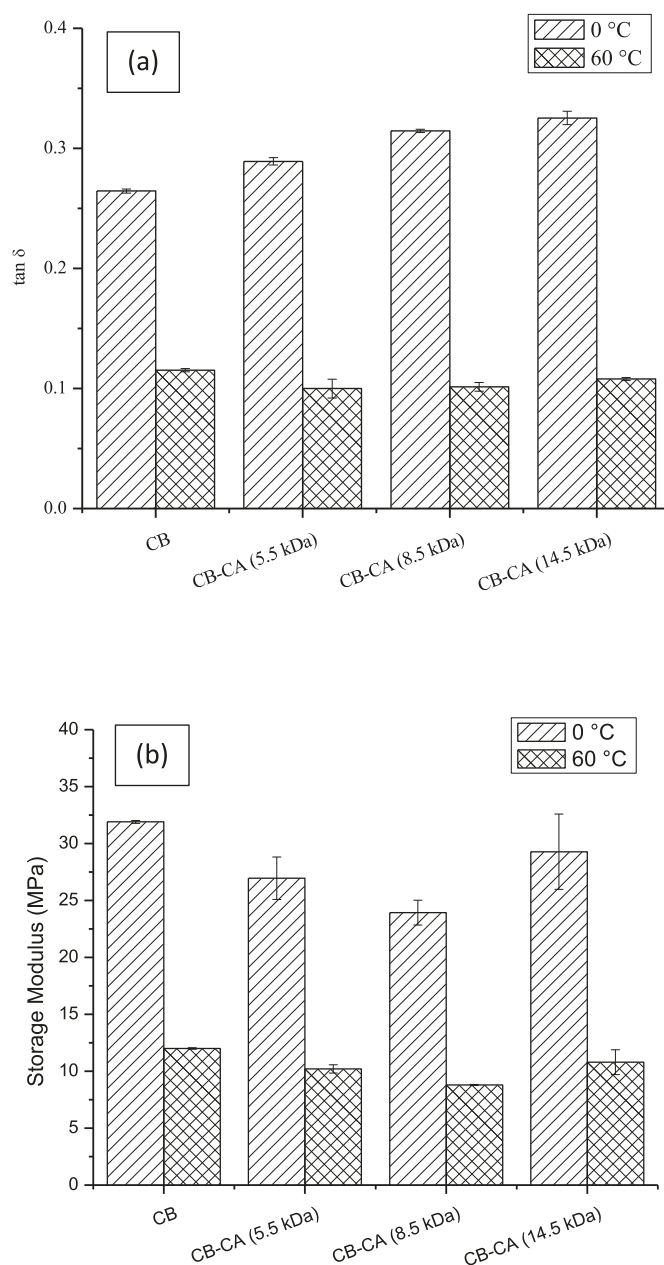


Fig. 11. Dynamic mechanical properties of rubber compounds with and without coupling agent: (a) rolling resistance indicator  $\tan \delta$ , and (b) storage modulus.

#### 4.9. Tensile properties of the compounds

The tensile strength and elongation at break values are shown in Fig. 12. Representative stress–strain diagrams are presented in Figure S3. The values of stress at 100% elongation (M100), 300% elongation (M300), and their ratios are included in Figure S4. The reduced stiffness caused by added CA also reduced the tensile strength values compared to the control as presented in Fig. 12(a). The elongation at break, however, is higher for materials containing coupling agents (Fig. 12(b)). It is apparent from the data presented in Figs. 11(b)–12 that the addition of CA resulted in a reduction of modulus values, but the extent of reduction is small at 14 kDa of molecular weight of the graft polymer.

The surface area of the filler significantly affects the reinforcement characteristics of filled elastomer compounds. Higher

structure and specific surface area leads to improved mechanical properties for CB filled rubber compounds [50,51]. As discussed earlier (Table 5), treatment of CB with the coupling agent reduced the BET surface area slightly. This change in surface area for modified CB particles might have resulted in reduced tensile strength for CA containing batches, compared to the control compound.

#### 4.10. Payne effect and filler flocculation

Filler networking in the cured system were estimated by studying filler flocculation at the same temperature used for rubber curing. The differences in flocculation behavior of carbon black and CA-coated carbon black particles were extracted from the dynamic mechanical properties, especially from the storage modulus, of the

uncured rubber compounds. Fig. 13(a)–(b) present the change in the storage modulus ( $G'$ ) versus time and percent strain, respectively. The increase in the storage modulus with time in Fig. 13(a) indicates that filler particles gradually flocculate and a filler network forms. The response of the storage modulus to applied strain in Fig. 13(b) is similar to what is observed for the Payne effect in cured rubbers. The Payne effect describes the non-linear decrease in the storage modulus with strain [52]; a larger decrease in the storage modulus corresponds to higher energy release with strain. Fig. 13(a) demonstrates that flocculation is much higher in the compound with untreated carbon black than that with CA-treated carbon black. Hence, the coupling agent significantly decreases flocculation of CB particles by van der Waals interactions. Fig. 13(b) demonstrates that the reduction of storage modulus values with strain is much lower in the compound with CA-treated carbon black than that with untreated carbon black. Thus, CB treated with CA shows reduced filler-filler interactions and hence a higher degree of micro-dispersion [53]. This indicates that the physical coupling agent used in this work is very useful at reducing filler networking and therefore lowering the rolling resistance in rubber compounds.

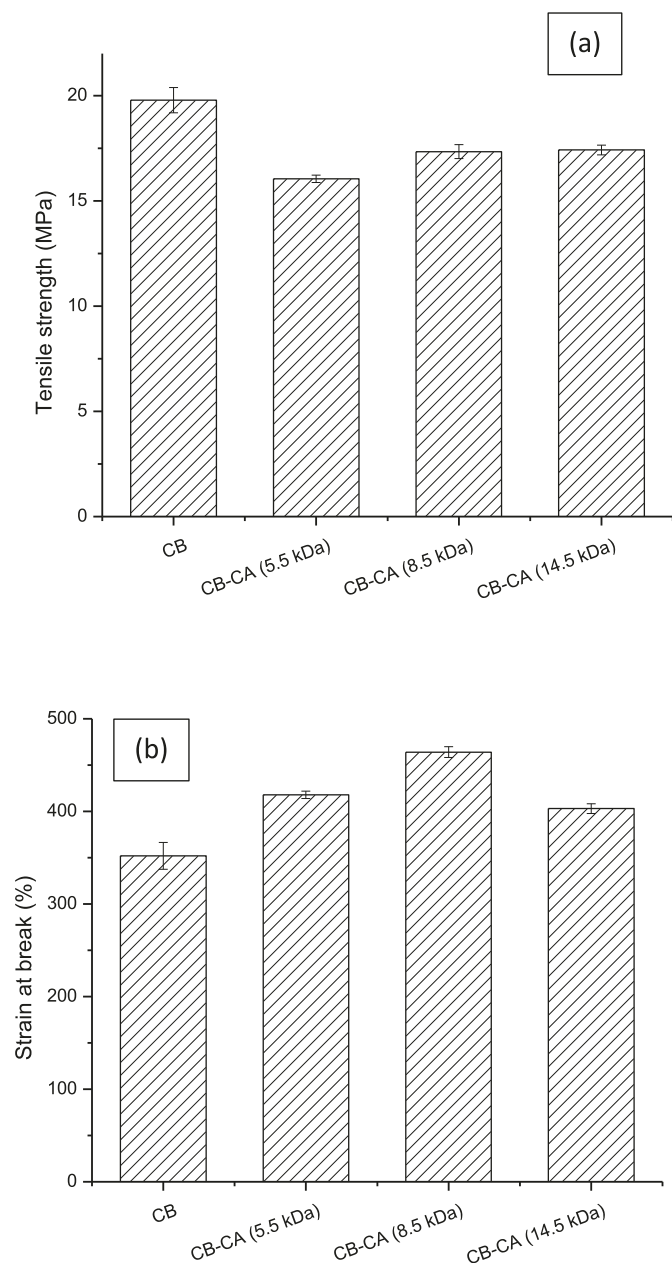


Fig. 12. Tensile strength (a), strain at break (b) for compounds with and without coupling agent.

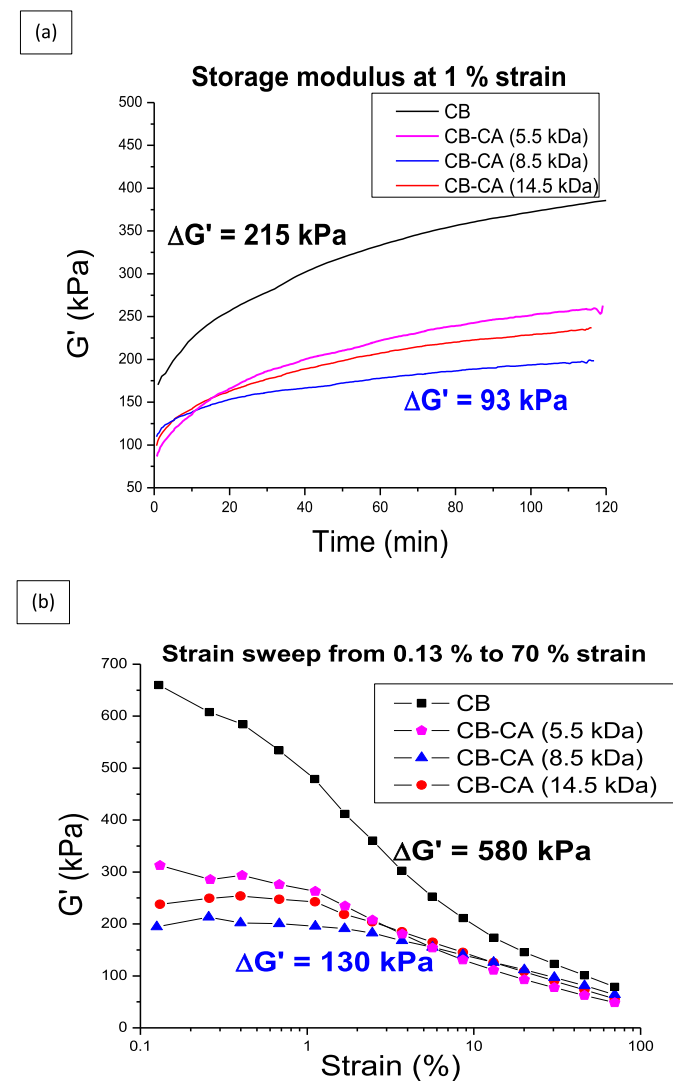


Fig. 13. (a) Filler flocculation and (b) analysis of the Payne effect of uncured rubber compounds with and without coupling agent.  $\Delta G'$  is the fit  $G'$  at the beginning minus  $G'$  at the end of the test sequence.

## 5. Conclusions

This work investigated the effectiveness of a coupling agent for CB dispersion in rubber compounds using arene-perfluoroarene interactions. The  $\pi$ - $\pi$  stacking interactions between electron-rich carbon black particles and the electron-poor pentafluorostyrene aromatic rings of PB-g-PPFS and PPFS were inferred from Raman spectroscopy. The morphology of the system changed due to the physical interactions between the CB particles and the coupling agent. A 35% reduction in the BET surface area and an increase in the zeta potential value of CB in CA solution indicated that adsorption of PB-g-PPFS graft copolymer onto CB particles occurred due to strong arene-perfluoroarene interactions. The cure kinetics of the vulcanizates were faster as a result of better dispersion of carbon black in the SBR matrix. Scanning electron microscopy confirmed the enhanced dispersion, evidently due to the use of the CA. The loss factor value at 60 °C was lower in all the compounds containing CA. The  $\tan \delta$  at 60 °C was reduced by 12% for the CA with graft  $M_n = 8.5$  kDa, and the wet traction increased as indicated by a higher  $\tan \delta$  value at 0 °C. Filler flocculation and Payne effect studies also confirmed the reduced energy loss in the case of compounds containing CA.

## Acknowledgments

This work was funded by CenTire (Center for Tire Research; joint between Virginia Tech and The University of Akron) and the National Science Foundation (Award IIP 1650460). We thank our CenTiRe industrial mentors for their collaboration and feedback on this work. We thank Robert Seiple and Dr. Crittenden Ohlemacher of The University of Akron for allowing access to the Applied Polymer Research Center's lab facilities.

## Appendix A. Supplementary data

Supplementary data related to this article can be found at <https://doi.org/10.1016/j.polymer.2018.06.025>.

## References

- [1] Department of Transportation, Tire Fuel Efficiency Consumer Information Program, 2010, 49 CFR Part 575 Docket No. NHTSA-2010-0036.
- [2] Transportation Research Board Special Report 286, Tires and Passenger Vehicle Fuel Economy, National Research Council of the National Academies, 2006. Docket No. NHTSA-2008-0121-0008.
- [3] M.-J. Wang, S. Wolff, J.-B. Donnet, Filler-elastomer interactions. Part III. Carbon-black-surface energies and interactions with elastomer analogs, *Rubber Chem. Technol.* 64 (1991) 714–736.
- [4] S. Wolff, M.-J. Wang, Filler-elastomer interactions. Part IV. The effect of the surface energies of fillers on elastomer reinforcement, *Rubber Chem. Technol.* 65 (1992) 329–342.
- [5] A. Klasek, J. Špaček, R. Čurík, S. Kafka, Efficiency of some novel carbon black/rubber coupling agents, *J. Appl. Polym. Sci.* 61 (1996) 1137–1146.
- [6] A.N. Gent, J.D. Walter, *Pneumatic Tire*, 2006, pp. 504–508.
- [7] M.-J. Wang, S. Wolff, E.-H. Tan, Filler-elastomer interactions. Part VIII. The role of the distance between filler aggregates in the dynamic properties of filled vulcanizates, *Rubber Chem. Technol.* 66 (1993) 178–195.
- [8] J.T. Byers, Silane coupling agents for enhanced silica performance, *Rubber World* 218 (1998) 38.
- [9] C.G. Robertson, C.J. Lin, R.B. Bogoslovov, M. Rackaitis, P. Sadhukhan, J.D. Quinn, C.M. Roland, Flocculation, reinforcement, and glass transition effects in silica-filled styrene-butadiene rubber, *Rubber Chem. Technol.* 84 (2011) 507–519.
- [10] N. Suzuki, F. Yatsuyanagi, M. Ito, H. Kaidou, Effects of surface chemistry of silica particles on secondary structure and tensile properties of silica-filled rubber systems, *J. Appl. Polym. Sci.* 86 (2002) 1622–1629.
- [11] S. Choi, J. Kim, J. Ko, Y.S. Cho, W.G. Shin, Influence of Coupling Agent on Properties of Carbon Black-reinforced SBR and NR/SBR Vulcanizates 13, 2007, pp. 1017–1022.
- [12] K.-J. Kim, J. Vanderkooi, Moisture effects on improved hydrolysis reaction for TESPT and TESPDS-silica compounds, *Compos. Interfac.* 11 (2004) 471–488.
- [13] L.A. Walker, J.J. D'Amico, D.D. Mullins, Nitrosoanilines. II, *J. Org. Chem.* 27 (1962) 2767–2772.
- [14] J.J. D'Amico, C.C. Tung, L.A. Walker, Nitrosoanilines, *J. Am. Chem. Soc.* 81 (1959) 5957–5963.
- [15] A.K. Ghosh, S. Maiti, B. Adhikari, Modified carbon black as reinforcing filler for SBR, *Indian J. Chem. Technol.* 4 (1997) 135–140.
- [16] T. Yamaguchi, I. Kurimoto, K. Ohashi, T. Okita, Novel carbon black/rubber coupling agent, *Kautsch. Gummi Kunstst.* 42 (1989) 403–409.
- [17] A. Klasek, E. Filipovicová, J. Špaček, Efficiency of some dinitrodiamines and dinitrodiamides in improving dynamic properties of vulcanized rubber, *J. Appl. Polym. Sci.* 81 (2001) 1439–1443.
- [18] N. Tsubokawa, K. Kobayashi, Y. Sone, Reactive carbon black having isocyanate or acyl azide group, *Polym. Bull.* 13 (1985) 215–222.
- [19] D.C. Havery, T. Fazio, Estimation of volatile N-nitrosamines in rubber nipples for babies' bottles, *Food Chem. Toxicol. Int. J. Publ. Br. Ind. Biol. Res. Assoc.* 20 (1982) 939–944.
- [20] K. Hattapanit, P. Sae-Oui, N. Sombatsompop, C. Sirisinha, Enhancement of rubber-carbon black interaction by amine-based modifiers and their effect on viscoelastic and mechanical properties, *J. Appl. Polym. Sci.* 126 (2012) E315–E321.
- [21] N. Tsubokawa, K. Kobayashi, Y. Sone, Grafting onto carbon black by the reaction of reactive carbon black having masked isocyanate or acyl azide group with functional polymers, *J. Polym. Sci. Part A Polym. Chem.* 26 (1988) 223–233.
- [22] C.R. Patrick, G.S. Prosser, A molecular complex of benzene and hexafluorobenzene, *Nature* 187 (1960) 1021.
- [23] A.F.M. Kilbinger, R.H. Grubbs, Arene-perfluoroarene interactions as physical cross-links for hydrogel formation, *Angew. Chem. Int. Ed.* 41 (2002) 1563–1566.
- [24] G.W. Coates, A.R. Dunn, L.M. Henling, D.A. Dougherty, R.H. Grubbs, Phenyl-perfluorophenyl stacking interactions: a new strategy for supermolecule construction, *Angew. Chem. Int. Ed.* 36 (1997) 248–251.
- [25] G.W. Coates, A.R. Dunn, L.M. Henling, J.W. Ziller, E.B. Lobkovsky, R.H. Grubbs, Phenyl-perfluorophenyl stacking interactions: topochemical [2+2] photodimerization and photopolymerization of olefinic compounds, *J. Am. Chem. Soc.* 7863 (1998) 3641–3649.
- [26] C. Dai, P. Nguyen, T.B. Marder, A.J. Scott, W. Clegg, C. Viney, Control of single crystal structure and liquid crystal phase behaviour via arene – perfluoroarene interactions, *Chem. Commun.* (1999) 2493–2494.
- [27] M.P. Cohen, R.M. D'Sidocky, Rubber chemicals, *Encycl. Polym. Sci. Technol* 11 (2004) 577–612.
- [28] M. Gerspacher, W. Wampler, J.T. Byers, Fillers, in: K.C. Baranwal, H.L. Stephens (Eds.), *Basic Elastomer Technol.*, First ed., The Rubber Division American Chemical Society, Akron, 2001, pp. 57–111.
- [29] A. Ciesielski, The basic rubber compound, in: *An Introd. to Rubber Technol.*, Rapra Technology Limited, Shawbury, Shrewsbury, Shropshire SY4 4NR, United Kingdom, 1999, pp. 31–48.
- [30] M. Paz-Pazos, C. Pugh, Synthesis, isolation, and thermal behavior of polybutadiene grafted with poly(2,3,4,5,6-pentafluorostyrene), *J. Polym. Sci. Part A Polym. Chem.* 43 (2005) 2874–2891.
- [31] K. Bahl, N. Swanson, C. Pugh, S.C. Jana, Polybutadiene-g-poly(pentafluorostyrene) as a coupling agent for lignin-filled rubber compounds, *Polymer* 55 (2014) 6754–6763.
- [32] J. Donnet, E. Custodero, Science and technology of rubber, in: F.R. Eirich (Ed.), *Sci. Technol. Rubber*, Elsevier, 2013, pp. 395–396.
- [33] S.-S. Choi, Difference in bound rubber formation of silica and carbon black with styrene-butadiene rubber, *Polym. Adv. Technol.* 13 (2002) 466–474.
- [34] S. Reich, C. Thomsen, Raman spectroscopy of graphite, *Philos. Trans. R. Soc. A Math. Phys. Eng. Sci.* 362 (2004) 2271–2288.
- [35] Y. Kameya, K. Hanamura, Kinetic and Raman spectroscopic study on catalytic characteristics of carbon blacks in methane decomposition, *Chem. Eng. J.* 173 (2011) 627–635.
- [36] K. Bahl, T. Miyoshi, S.C. Jana, Hybrid fillers of lignin and carbon black for lowering of viscoelastic loss in rubber compounds, *Polymer* 55 (2014) 3825–3835.
- [37] M.A. Pimenta, G. Dresselhaus, M.S. Dresselhaus, L.G. Cançado, A. Jorio, R. Saito, Studying disorder in graphite-based systems by Raman spectroscopy, *Phys. Chem. Chem. Phys.* 9 (2007) 1276–1290.
- [38] G. Katagiri, H. Ishida, A. Ishitani, Raman spectra of graphite edge planes, *Carbon N. Y.* 26 (1988) 565–571.
- [39] Y. Liu, L. Gao, J. Sun, Noncovalent functionalization of carbon nanotubes with sodium lignosulfonate and subsequent quantum dot decoration, *J. Phys. Chem. C* 111 (2007) 1223–1229.
- [40] J.T. Byers, Filler Part I: carbon black, in: M. Morton (Ed.), *Rubber Technol.*, third ed., Springer Science & Business Media, 2013, pp. 67–68.
- [41] R. Xu, C. Wu, H. Xu, Particle size and zeta potential of carbon black in liquid media, *Carbon N. Y.* 45 (2007) 2806–2809.
- [42] H.M. da Costa, L.L.Y. Visconte, R.C.R. Nunes, C.R.G. Furtado, Rice-husk-ash-filled natural rubber. II. Partial replacement of commercial fillers and the effect on the vulcanization process, *J. Appl. Polym. Sci.* 87 (2003) 1405–1413.
- [43] P.K. Pal, A.K. Bhowmick, S.K. De, The effects of carbon black-vulcanization system interactions on natural rubber network structures and properties, *Rubber Chem. Technol.* 55 (1982) 23–40.
- [44] M. Porter, Structural characterization of filled vulcanizates part 1. Determination of the concentration of chemical crosslinks in natural rubber vulcanizates containing high abrasion furnace black, *Rubber Chem. Technol.* 40

- (1967) 866–882.
- [45] Z.H. Li, J. Zhang, S.J. Chen, Effects of carbon blacks with various structures on vulcanization and reinforcement of filled ethylene-propylene-diene rubber, *Express Polym. Lett.* 2 (2008) 695–704.
- [46] A.Y. Coran, Vulcanization, in: J.E. Mark, B. Erman, M. Roland (Eds.), *Sci. Technol. Rubber*, Academic press, 2013, pp. 362–364.
- [47] N. Tricàs Rosell, *Plasma Modification on Carbon Black Surface: from Reactor Design to Final Applications* (Ph.D. thesis), Universitat Ramon Llull, 2007, <http://hdl.handle.net/10803/9288>.
- [48] A.F. Halasa, B.B. Gross, W.-L. Hsu, Multiple glass transition terpolymers of isoprene, butadiene, and styrene, *Rubber Chem. Technol.* 83 (2010) 380–390.
- [49] H. Takino, R. Nakayama, Y. Yamada, S. Kohjiya, T. Matsuo, Viscoelastic properties of elastomers and tire wet skid resistance, *Rubber Chem. Technol.* 70 (1997) 584–594.
- [50] M. Bhattacharya, A.K. Bhowmick, Synergy in carbon black-filled Natural rubber nanocomposites. Part I: mechanical, dynamic mechanical properties, and morphology, *J. Mater. Sci.* 45 (2010) 6126–6138.
- [51] O.A. Al-Hartomy, F. Al-Solamy, A. Al-Ghamdi, N. Dishovsky, M. Ivanov, M. Mihaylov, F. El-Tantawy, Influence of carbon black structure and specific surface area on the mechanical and dielectric properties of filled rubber composites, *Int. J. Polym. Sci.* 2011 (2011).
- [52] G. Heinrich, M. Klüppel, T.A. Vilgis, Reinforcement of elastomers, *Curr. Opin. Solid State Mater. Sci.* 6 (2002) 195–203.
- [53] N. Tokita, M.J. Wang, B. Chung, K. Mahmud, Future carbon blacks and new concept of advanced filler dispersion, *Nippon Gomu Kyokaishi* 71 (1998) 522–533.